Int. J. Heat Mass Transfer. Vol. 22, pp. 61–75
Pergamon Press Ltd. 1979 Printed in Great Britain

ELECTRO-CHEMICAL MEASUREMENTS OF MASS TRANSFER IN SEMI-CYLINDRICAL HOLLOWS

J. K. AGGARWAL* and L. TALBOT†

(*Received* 6 *December* 1976 *and in revised form* 24 *April* 1978)

Abstract—Measurements are described of the circumferential distribution of local Sherwood number in a semi-cylindrical hollow oriented transverse to the main flow in the base of a narrow rectangular channel. This geometry, among other reasons, is of interest because of its application to blood oxygenation equipment. The experimental arrangement was such that hydro-dynamically fully-developed laminar flow existed at entry to the hollow, and measurements covered a Reynolds number range of about 20–500 based on the hollow diameter and channel mean velocity. An electro-chemical technique, in which a redox couple comprised the electrolyte and thin nickel wires formed the test electrodes, was utilized. Current measurements, made under conditions of diffusion-controlled electrolytic reaction, led to the evaluation of the Sherwood number. The circumferential distribution of Sherwood number within the hollow as a function of the Reynolds number of flow and the hollow size are presented in graphical form. Sherwood number increased with both the Reynolds number and the hollow diameter, but it usually exhibited a minimum somewhere in the upstream quadrant of the hollow. The Sherwood number, averaged over the hollow circumference, was computed and yielded a correlation identical to the one in the absence of the hollow, except for a smaller value of the constant. The results were compared with a numerical calculation by Snuggs and Aggarwal of the Sherwood number distribution in the hollow and were found to be in excellent agreement.

NOMENCLATURE

a, exponent in equation (16);
b, channel half-height;
c, concentration of the reacting species;
c_f, local wall skin friction coefficient $(= 2\tau/\rho u_m^2)$;
$\bar{c}_f$, average wall skin friction coefficient;
c_0, bulk concentration;
c_s, surface concentration;
D, molecular diffusivity of the reacting species;
d, diameter of the hollow;
d_e, diameter of electrode;
F, Faraday's constant $(= 96\,494\,\text{C})$;
i, current density;
i_l, limiting current density;
K, function of d in equation (12);
k, local mass-transfer coefficient for isolated electrode;
$\bar{k}$, average of local mass-transfer coefficients;
L, electrode length;
$\dot{m}$, mass flux normal to electrode surface;
n, valence charge of an ion;
R, gas constant;
Re, Reynolds number;
Sc, Schmidt number $(= \nu/D)$;
Sh, Sherwood number in the hollow $(= kd/D)$;
Sh_0, Sherwood number in the absence of hollow $(= kb/D)$;
$\overline{Sh}$, spatial-averaged Sherwood number;
s, time-averaged velocity gradient;
T, absolute temperature;
t, time (also dummy variable);
u, velocity component in the x-direction;
u_m, mean velocity of flow in channel;
v, velocity component in the y-direction;
w, width of electrode;
x, co-ordinate in the flow direction;
y, co-ordinate perpendicular to the electrode surface;
z, co-ordinate in the direction of electrode width.

Greek symbols

δ_m, diffusion-layer thickness;
ε_m, eddy-diffusivity of mass;
ε_ψ, eddy-diffusivity of electrostatic potential;
θ, angular position within the hollow, measured from its upstream lip;
μ, dynamic viscosity of fluid;
ν, kinematic viscosity of fluid;
ρ, fluid density;
τ, wall shear stress in the hollow;
τ_0, wall shear stress in the absence of hollow;
ψ, electrostatic potential.

Subscripts

b, quantity based on channel height;
d, quantity based on the hollow diameter.

*Department of Engineering Science, Oxford University, England.
†Mechanical Engineering Department, University of California, Berkeley, U.S.A.

1. INTRODUCTION

THERE exists a continuing search for more compact and more efficient blood oxygenators or artificial

lungs capable of prolonged extra-corporeal assistance with minimum amount of blood trauma. In one of their simplest forms, oxygen is bubbled through a column of blood. Although bubble oxygenators have been widely used in open heart surgery, they cause significant haemolytic changes and thereby seriously limit perfusion times. A membrane lung device, in which a silicone membrane is interposed between blood and oxygen, is less traumatic and consequently more suited to prolonged perfusion without decreased function [1–3]. Its effectiveness is controlled by the mechanism of the transport of oxygen (similar considerations apply to the transport of CO_2 but in the opposite direction) from the membrane surface to the blood stream and by the membrane properties, the latter not being the concern of this study. The transfer of oxygen across a lung device membrane and its associated boundary layer is mainly limited by the concentration gradient driving the diffusional transport of oxygen. Owing to the poor solubility of oxygen in plasma, an oxygenator employing diffusional transport requires a large membrane surface area to achieve adequate respiratory oxygen exchange, making difficult the achievement of compactness of the device.

An extremely effective method of enhancing oxygen transport is the utilization of convective mixing; thus red cells saturated with oxygen are transported to oxygen-poor regions of the flow while unsaturated red cells are carried to oxygen-rich areas. That convective mixing by secondary motion can effectively augment mass-transfer processes in heat exchangers and chemical reactors has long been known but its application in the design of membrane oxygenators is only recent [4, 5]. Secondary flow can be induced by oscillating either the channel carrying the blood or the blood itself. An example of the former arrangement is a fluid-filled torus driven in torsional oscillation about its axis of curvature [7] in which blood was forced sequentially through a series of toroidal membrane passages and good oxygen transfer was achieved. It was claimed that the oxygenator performance was not limited by gas diffusion in the blood phase, i.e. the blood mixing was complete. However, the oxygenator was fairly large in size and complex machinery was required to oscillate the device. Bellhouse *et al.* [8, 9] used a furrowed membrane (with furrows oriented transverse to the flow direction) and oscillated the blood flow. In forward flow, strong vortices formed convectively (i.e. due to fluid flowing in and out of furrows). During flow reversal, these vortices were ejected from the furrows and replaced by sets of contra-rotating vortices. This produced good mixing.

Good mixing can also be achieved by using very narrow channels, for instance, in the form of capillary tubes; this has the desired effect of increasing the surface to volume ratio, thereby reducing the prime volume of the device. However, the power required to drive the blood increases considerably. If the flow is made turbulent, good convective mixing occurs but at the expense of high intensity shear regions unfavourable to blood and to the arterial wall [10]. Convective mixing in laminar flows can be induced simply by using irregular membrane surfaces. Weissman and Mockros [4] have claimed that if the blood flows through a helically-coiled tube, gas-transfer rates up to a hundred times greater than that for a comparable straight tube can be achieved, provided the flow parameters are optimized. This phenomenal improvement in gas transfer is ascribed to the secondary mixing of the fluid in the cross-sectional plane of the tube due to the twin contra-rotating helical vortices generated by the centrifugal forces. Other studies of flow in curved tubes have reported much more modest increases in heat and mass transfer. Kolobow *et al.* [1] found that by exposing the blood to a rough membrane surface, it was possible to increase the efficiency of their spiral membrane oxygenator by 100% or more. In fact, the use of roughened surfaces to augment convective heat and mass transfer such as in advanced gas-cooled reactors, has long been exploited as a powerful tool [11].

The present study is concerned with the use of vortex-type flows, created by furrowed passages, to enhance mass transfer at the walls of a channel, under laminar flow conditions. The overall performance of a membrane oxygenator utilizing furrowed channels to enhance oxygen transfer has already been evaluated by Bellhouse [8], when the blood flow was oscillated at a frequency of 100/min. The parameters governing the oxygenator performance were chosen on the basis of dye visualization experiments. Therefore, detailed information on the distribution of mass transfer within a single hollow is thus far lacking, not only for the case of pulsatile flow, but even for the simpler case of steady flow, the understanding of which would seem to be a prerequisite for the study of the pulsatile flow case.

In this paper, experimental measurements are reported of local isolated mass-transfer coefficients within a single transverse semi-cylindrical hollow located in the lower wall of a narrow channel, when the flow in the channel at entry to the hollow is steady, laminar and fully-developed. The channel cross-section was 80×10 mm and the hollow diameter ranged from 4 to 12 mm. The Reynolds number of flow, based on the channel mean velocity and the hollow diameter, varied from about 20 to 500. The measurements were made at nine test electrodes (only six electrodes in the case of 4 mm dia hollow) equispaced around the periphery at centre span.

The electro-chemical technique was employed for these measurements. In this method, a cathode is mounted flush with the surface at the desired location and a larger anode is mounted downstream. The rig is perfused with an electrolyte which comprises a redox couple containing a large excess of

a supporting electrolyte. The magnitude of DC potential applied between the electrodes is such that a diffusion-controlling electrolytic reaction takes place. Under these conditions, the resulting DC current is readily related to the mass-transfer coefficient at the surface.

The distribution of Sherwood number around the hollow circumference is presented over an extensive range of flow rates and for five different hollow sizes. Local as well as average Sherwood numbers have been computed. An empirical correlation for the average Sherwood number over the hollow periphery is proposed and it is found that this relationship is independent of the hollow diameter. The local Sherwood number has also been calculated numerically and found to be in very good agreement with the experimental data.

2. PRINCIPLE OF THE ELECTRO-CHEMICAL MEASUREMENT OF MASS TRANSFER

An electrolytic reaction is caused to occur between two nickel electrodes—a small test cathode mounted flush with the channel wall at the point of measurement and a large anode mounted downstream. The test rig is filled with an electrolytic solution which, in the present work, consisted of equimolar concentrations (0.01 M) of potassium ferro- and ferricyanides mixed with an excess of a carrier electrolyte (1.0 M of sodium hydroxide). The following reactions occur under the influence of a DC potential applied between the electrodes:

At the cathode $Fe(CN)_6^{3-} + e \rightarrow Fe(CN)_6^{4-}$

At the anode $Fe(CN)_6^{4-} \rightarrow Fe(CN)_6^{3-} + e.$

This redox reaction at nickel electrodes is chosen [12] in preference to solid dissolution or deposition reactions because: (a) the surface remains smooth and physically unaltered, (b) the reaction occurs with negligible chemical polarization and (c) the frequency response is higher.

As ions of a reacting species are transferred from the bulk of the solution to the electrode surface, a concentration gradient is set up. In the steady state, the rate of mass transfer per unit area, $\dot{m}$, perpendicular to the electrode surface (i.e. in the y-direction) is given by

$$\dot{m} = (D+\varepsilon_\psi)c(n/RT)\partial\psi/\partial y - (D+\varepsilon_m)\partial c/\partial y + vc. \quad (1)$$

The three terms on the RHS of equation (1) represent respectively migration due to the potential field, diffusion due to the concentration gradient and convection due to the flow. Owing to the high electrical conductance of the unreactive electrolyte (sodium hydroxide), the migration term can be neglected. Further, there is no net bulk flow transverse to the electrode surface; so the convective term disappears. Equation (1) thus reduced to

$$\dot{m} = -(D+\varepsilon_m)\partial c/\partial y$$

the negative sign accounting for the fact that the mass transfer to the wall is in the negative y-direction. On integration, one obtains

$$\dot{m} = -k(c_0 - c_s) \quad (2)$$

where the subscripts 0 and s refer to the bulk and surface conditions respectively, and k is the mass-transfer coefficient defined as

$$k = \frac{D+\varepsilon_m}{\delta_m}$$

where δ_m is the diffusion-layer thickness according to the concept of Nernst [13]. In all the studies reported here, the flow was laminar, so ε_m was taken to be zero.

Faraday's first law relates the mass flux at the electrode to the resulting current density, i, viz.

$$\dot{m} = -i/nF. \quad (3)$$

For the reduction of ferricyanide considered here, $n = 1$. Combining equations (2) and (3), one obtains

$$k = i/F(c_0 - c_s). \quad (4)$$

Thus, the mass-transfer coefficient, k, can be calculated from experimental measurements, provided c_s is known. Two assumptions will now be made: (a) the process is reversible, i.e. the reaction is so rapid that electro-chemical equilibrium is achieved at the electrode surface and kinetics of electron transfer can be ignored; (b) the ferricyanide concentration is independent of current and time in the steady-state implying that the rate of mass transfer is much larger than the rate of electrochemical reaction. These assumptions are plausible for the redox couple chosen.

As the negative potential applied to the cathode is increased, the current increases until a state is reached when the ferricyanide ions react at the surface at a rate equal to their maximum rate of transport to the surface, i.e. $c_s \rightarrow 0$. The current then asymptotes to a value (the limiting current) which remains constant despite further increase in the applied potential, until a second regime is reached when hydrogen liberation from the cathode causes a further increase in current. All experiments described in this paper were performed under limiting current conditions in the absence of hydrogen liberation; k is thus obtained from the simplified version of equation (4), namely

$$k = i_l/Fc_0. \quad (5)$$

The non-dimensional mass-transfer coefficient, the Sherwood number Sh, can be expressed as

$$Sh = \frac{kd}{D} = i_l d/Fc_0 D \quad (6)$$

where d is a characteristic dimension.

Further details of this technique are given by Reiss and Hanratty [14, 15] who made measurements of fluctuating mass transfer in the vicinity of a pipe wall in order to study the unsteady nature of the viscous sublayer.

3. EXPERIMENTAL EQUIPMENT AND TECHNIQUE

A schematic representation of the recirculating tunnel used in the present study appears in Fig. 1. The electrolytic solution entered from a constant-head header tank via a bell-mouth into the test-section which was rectangular in cross-section −80 mm wide and 10 mm high. The velocity profile at entry to the test-section was laminar and fully developed throughout the range of Reynolds number encountered in the tests [16], since a length equal to 70 channel heights was provided upstream of the test-section. The top and bottom plates of the test-section could be removed readily for ease of inspection and completely encased by a wooden enclosure which was covered with black polythene with provision for access through the front. The test solution was thus shielded from light for the most part of an operating day. Measurements made on the reference electrode indicated that the same solution could be used for a full working week with little degradation in the ferricyanide concentration.

3.1. *The electrodes*

All electrodes were made of nickel and were mounted flush with the local surface. The top plate of the test-section incorporated a circular reference

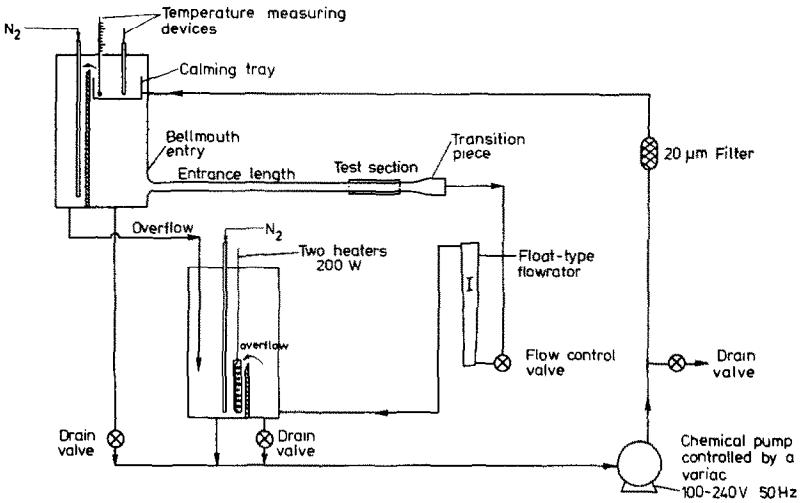

FIG. 1. Schematic arrangement of the rig.

interchangeability. Test sections containing semi-cylindrical hollows transverse to the flow of diameters ranging from 4 to 12 mm were installed in the bottom plate. The bottom plate was chosen in order to provide for easy escape of any gas bubbles entrained in the solution and trapped in the test section.

The flow rate was measured by a float-type flow meter (Model 10A 3565, Fischer and Porter, Workington, Cumberland). This was previously calibrated using a bucket and stop-watch. The solution was collected, via a control valve, by a constant-head dump tank and was then pumped back into the header tank. The flow rate through the pump was varied by controlling its speed through a Variac. An "Intersept" transfusion blood filter (made by Johnson and Johnson, New Jersey, U.S.A.) was introduced in the pump circuit to remove all undesirable debris over 20 μm in size and to exclude gas bubbles in suspension. The filter element is woven from polyester monofilaments and is enclosed in a cylindrical polypropylene housing.

The test-section and the tanks were fabricated from perspex, and polythene tubing was used throughout. Tests were carried out to ensure that all components of the rig were constructed from materials inert to the electrolyte. The test rig was electrode of 0.52 mm dia mounted upstream and a larger rectangular anode 12 mm long and 80 mm wide mounted at the most downstream location. The anode was made much larger than any of the cathodes so that under normal operating condition the circuit current was not limited by the anode but was controlled by diffusion at the cathode. All the test electrodes (i.e. cathodes) were circular and of 0.5 mm nominal diameter. Figure 2 depicts the positions of the axes of such electrodes mounted in

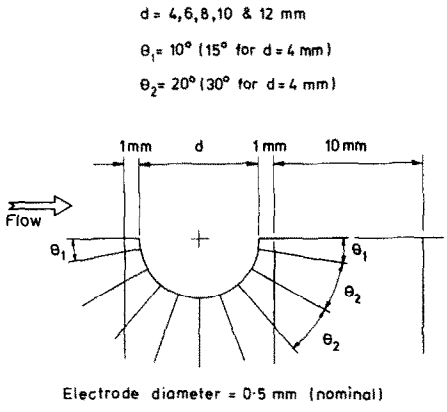

FIG. 2. Positions of test electrodes.

and around the hollow at mid-span. A number of electrodes were equispaced round the periphery and a few were mounted on the flat portion of the channel. In addition four electrodes were mounted along the bottom generator of the hollow and spaced to cover the entire span.

As it is imperative that the electrodes be implanted absolutely flush with the wall, it is perhaps appropriate to mention the difficulties encountered in the mounting procedure. Initially, the following technique was employed. A circular hole of diameter equal to that of the electrode was drilled in the plastic plate and the electrode was passed through the hole (thus giving an "interference" fit) until it just protruded from the wall. The electrode end was then ground, by hand, flush with the wall. However, stresses developed in the region around the electrode surface gave rise to tiny cracks in the plastic, which eventually resulted in the formation of small pockets and craters around the electrodes, presumably due to attack by the solution which seeped into the stress cracks. To eliminate this problem, the following method was employed for electrodes mounted on the flat surface. A hole of slightly larger diameter than that of the electrode was drilled, the electrode was accurately aligned centrally within the hole and the gap was carefully filled with an acrylic cement (Tensole No. 7, I.C.I.) as shown in Fig. 3. After the cement was fully cured, the electrode surface was buffed with progressively finer grades of emery and was finally lapped with wetted 3 μm powder of aluminium oxide.

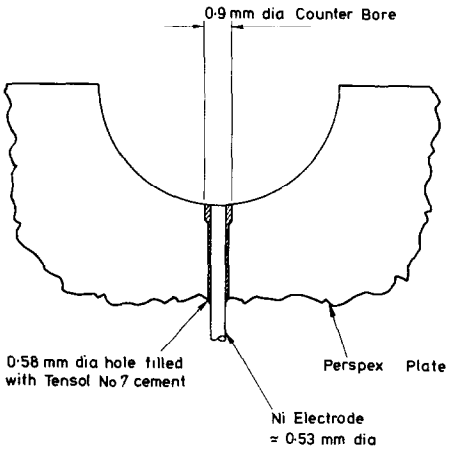

FIG. 3. Mounting of an electrode.

A slightly different procedure was adopted for the electrodes mounted inside the hollow. Initially, the size of the hollow cut was slightly smaller than the required size. After all the electrodes were mounted flush, the hollow was finally machined to the correct size and polished with wetted aluminium oxide powder. This technique proved to be quite satisfactory, although after many months of constant usage, slight etching of the cementing material around several electrodes was observed.

Prior to any runs, the electrode surface was buffed with soft tissue and cleaned with distilled water to ensure that no oxide film was present on the surface. It was found that the normally recommended cathodic treatment [17] at a current density of 20 mA cm^{-2} for 10–20 min in a 5% NaOH solution did not alter the results.

The projected diameter of each electrode was measured to an accuracy of 0.001 mm using a travelling microscope, the axis of viewing being coincident with the electrode axis. This diameter was used to calculate the surface area of the electrode; the error introduced by the curvature of the hollow was less than 0.3% in the worst case of the smallest hollow of 4 mm dia. Also, the surface roughness in the immediate vicinity of each mounted electrode was measured using a "Taylor–Hobson" profilometer and it was found to be an order of magnitude smaller than the estimated thickness of the concentration boundary layer.

3.2. *The electrolytic solution*

The electrolyte used in the present experiments consisted of the following mixture:

0.01 M of potassium ferrocyanide, $K_4Fe(CN)_6$,
0.01 M of potassium ferricyanide, $K_3Fe(CN)_6$, and
1.0 M of sodium hydroxide, NaOH.

The prime volume of the test rig was under 9 l; appropriate quantities of the chemicals were weighed by an electronic balance accurate to 0.1 mg and dissolved in distilled water. As the limiting current measured is directly proportional to the bulk concentration of ferricyanide ions, it is important to know this concentration accurately. The slow photochemical decomposition of $K_4Fe(CN)_6$ to hydrogen cyanide contaminates the solution in addition to poisoning the electrode surface:

$$Fe(CN)_6^{4-} + H_2O \underset{\text{dark}}{\overset{\text{light}}{\rightleftharpoons}} Fe(CN)_5^{3-} + CN^-$$

$$CN^- + H_2O \rightleftharpoons HCN + OH^-.$$

In view of this, volumetric analysis using an idometric method was performed daily to monitor the ferricyanide concentration in the solution. The procedure used is similar to that described by Swift [18].

As the property values, and in particular the diffusivity of the electrolyte, are dependent upon the temperature, it was decided to maintain the temperature of the fluid constant at 25°C. This was achieved to within ±0.2°C by immersing in the solution two 200 W glass-encapsulated cylindrical heaters in the dump tank and using a "Nobel" proportional controller. In order to release any dissolved air from the solution prior to any runs, nitrogen was bubbled through the electrolyte until the solution was saturated with nitrogen. Bubbling of nitrogen was continued throughout all the runs. This achieved a two-fold objective of avoiding the possible oxidation of ferrocyanide and of eliminating the side reaction

involving the reduction of dissolved oxygen at the cathode, namely $O_2+2H_2O+4e \rightarrow 4OH^-$, which would otherwise contribute to the measured current. Further, if the alkaline solution is exposed to air, it may absorb hydrogen sulphide with consequent introduction of chemical polarisation.

The property values for the electrolyte were calculated using semi-empirical equations well summarized by Gordon *et al.* [19]. When the density of a sample solution was measured using a $10\,cm^3$ pycnometer calibrated to British Standard, it was found to be within 0.25% of the calculated value using the polynomial equations given in [19].

3.3. *Current measurement*

It was found from experimental polarization curves, depicted in Fig. 4 at two extreme and two intermediate rates of flow, that saturation current

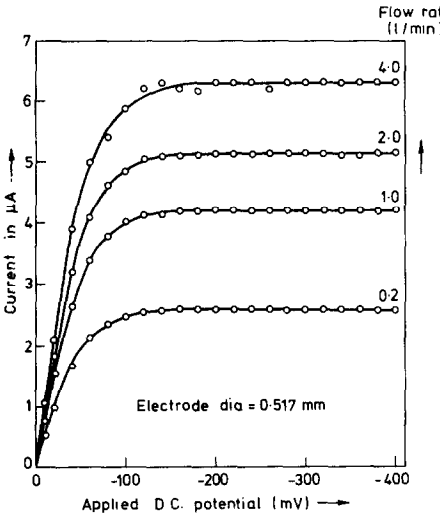

FIG. 4. Polarization curves for the reduction of ferricyanide.

plateau always occurred at anode potentials above 200 mV. As all the experiments were performed under limiting current conditions, it was essential to keep the voltage across the electrodes at a fixed value; this was chosen to be 250 mV. Since the total supply voltage was also constant, an electronic circuit was developed to maintain the electrode voltage constant independent of the current. The basic element of the circuit is the control operational amplifier, which maintains the voltage across the "electrochemical probe" equal to the selected reference voltage, independent of the current passing through the probe. The current is determined by measurement of the potential drop across the selected feedback resistor, using a voltage follower amplifier and differential (subtractor) amplifier together with the two voltage dividers. Current could be measured over the range of 10 μA to 10 mA full scale. Figure 5 shows a simplified version of the circuit.

It is worth noting that a large signal containing harmonics of the mains frequency as well as some white noise was superimposed on the output signal. Further, this stray signal was extremely sensitive to external electrical disturbances such as turning on or off of electrical equipment or lights. It was concluded that the large anode in conjunction with the conducting electrolyte acted as an antenna for this signal. When the anode was run at zero (i.e. earth) potential and the cathode was operated at negative 250 mV potential, this signal disappeared completely!

4. MEASUREMENTS IN THE ABSENCE OF HOLLOW

The first series of experiments was performed to establish that the flow at entry to the channel was fully-developed and to determine the accuracy of the technique and prove the rig generally. A total of six different electrodes, all of the same nominal diameter $d_e = 0.52$ mm and spaced at various distances from the entry section, were installed in the bottom flat plate and measurements of current under the limiting current conditions were made with Reynolds number $Re_b = 2u_m b/\nu$ based on channel height $2b$ and the mean velocity u_m varying in the range 7–1000. The current density values (measured current divided by the surface area of the particular electrode) were plotted against Reynolds number for all the electrodes. This variation is depicted in Fig. 6 for a typical electrode but in fact there was virtually no scatter (less than 1%) between the electrodes. The experimental points exhibit a linear variation except at very low Reynolds number where the measured values are slightly higher because of contribution

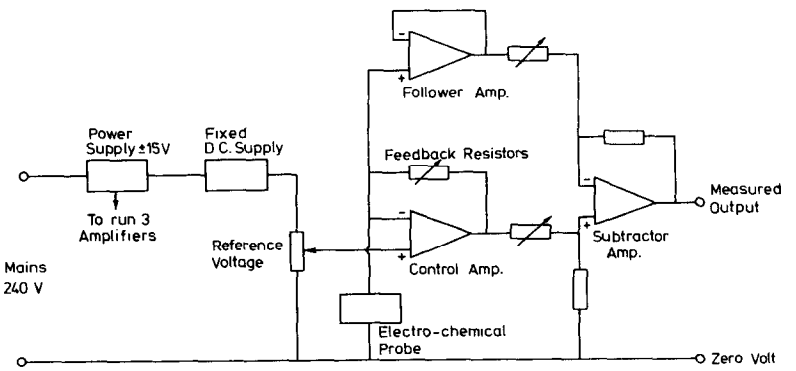

FIG. 5. Simplified electronic circuit diagram.

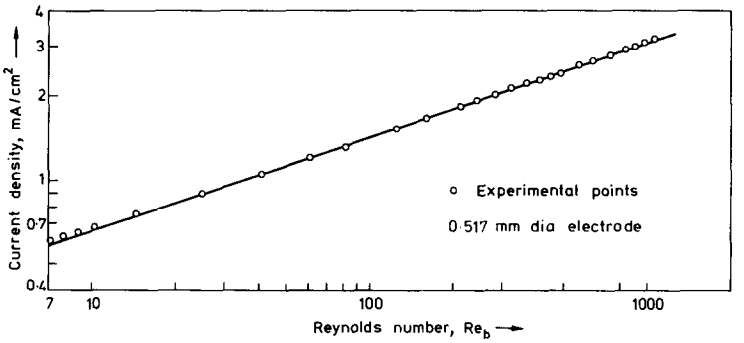

FIG. 6. Current density in fully-developed channel flow.

from: (a) diffusion in the direction of flow, and (b) natural convection due to density differences in the concentration boundary layer.

This confirmed that the flow was fully-developed at entry to the test section. Further, tests carried out earlier with dye injection showed that the flow was laminar, and two-dimensional over at least the middle-half span.

A rectangular strip electrode of length $L = 3$ mm in the flow direction and spanning the full width of the channel (80 mm) was mounted flush in the bottom plate and current measurements were made over the full range of Reynolds number. The Sherwood number, Sh_b, was calculated from the following relationship,

$$Sh_b = kb/D \tag{7}$$

and the mass-transfer coefficient, k, was computed with the aid of equation (5) in which the bulk ferricyanide concentration, c_0, was determined by titration. Experimental values of Sherwood number are plotted against Reynolds number and these are depicted as circles in Fig. 7. Also plotted on this figure is a theoretical equation which is described in the following sub-section.

4.1. *Mass transfer in fully-developed channel flow*

Consider a rectangular electrode of length $L \ll w$, its width, embedded flush with the channel wall. The concentration boundary layer will therefore be very thin and two-dimensional. It will thus be reasonable to assume that the velocity gradient in the concentration boundary layer is linear. Define x and y as the co-ordinate axes in the flow direction and perpendicular to the electrode surface respectively and u and v as the corresponding velocity components. The flow will be assumed uniform over the electrode surface so that u and v are not dependent upon x or z (z being in the direction of the electrode width). For the redox system of ferro-ferricyanide used, mass balance for the ferricyanide ion gives

$$\frac{\partial c}{\partial t} + u\frac{\partial c}{\partial x} + v\frac{\partial c}{\partial y} = D\frac{\partial^2 c}{\partial y^2}. \tag{8}$$

The axial diffusion term has been neglected because, in the present experiments $sL^2/D > 5000$ and Ling [20] has shown this to be valid. The appropriate boundary conditions along with the solution of equation (8) can be found in [17]. It is shown that if k represents the average mass-transfer coefficient over the electrode surface, then the time-averaged velocity gradient at the wall, s, assumed constant over the length L of the electrode, is given by

$$s = 1.8989k^3L/D^2. \tag{9}$$

The wall shear stress in fully-developed channel flow is given by the equation

$$\tau_0 = 3u_m\mu/b = s\mu. \tag{10}$$

Equations (9) and (10) can be combined and arranged to give the fully-developed channel flow Sherwood number,

$$Sh_0 = kb/D = 0.9244(Re_bScb/L)^{1/3} \tag{11}$$

in which $Sc = v/D$ is the Schmidt number.

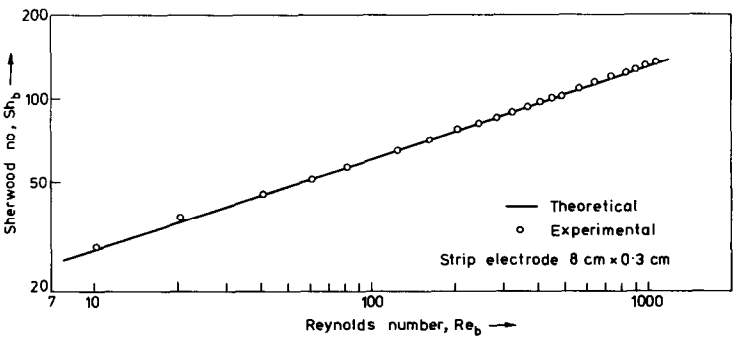

FIG. 7. Sherwood number for a strip electrode.

This equation, which is the same as Lévêque's equation when modified for mass transfer, is seen plotted in Fig. 7 as the theoretical line and it is in excellent agreement with the experiment. It is estimated that the overall accuracy of any measurement is well within 3%. Since both the circular electrode mounted at the midspan of the channel (Fig. 6) and the strip electrode which spanned the entire width of the channel (Fig. 7) gave results in excellent agreement with the two-dimensional Lévêque theory, it may be concluded that three-dimensional effects due to the channel side walls had a negligible influence on the measurements. (For the circular electrode, it can be shown [17] that in equation (11) $L = 0.8136 d_e$, where d_e is the electrode diameter.)

5. RESULTS

Following establishment of the accuracy of the method, tests were carried out in the hollow with the electrodes equi-spaced around the circumference at centre span. Five hollow sizes were studied – 4, 6, 8, 10 and 12 mm dia – and current measurements under mass-transfer-controlled conditions were made with a fully-developed velocity profile at entry; the Reynolds number of flow, Re_b, was varied from about 40 to 400 in ten nearly equal steps. Measurements made on the four additional electrodes installed along the bottom generator of the hollow at locations intermediate between the side walls and the centre of the channel showed that there was little variation between their outputs, thus confirming the conclusions of the dye observations and the comparison between the strip and circular electrodes in the absence of a hollow that the flow was two-dimensional over at least the middle half-span. All of the local Sherwood number measurements within the hollow were made at the midspan location, and thus can be considered reliably to represent two-dimensional flow values.

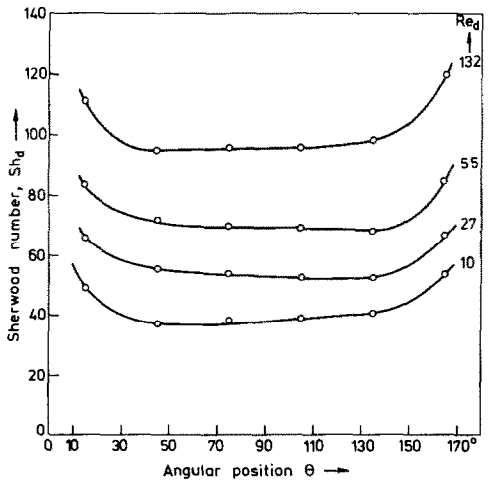

FIG. 8. Circumferential variation of Sherwood number, $d = 4$ mm.

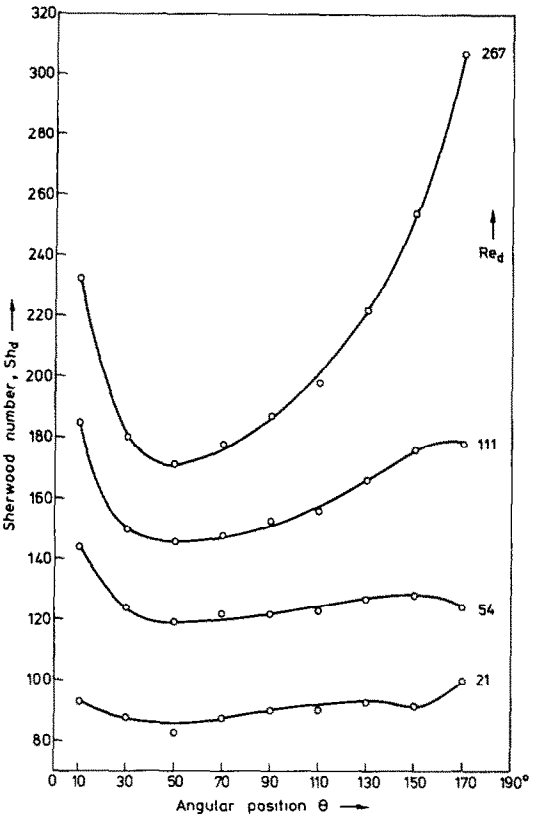

FIG. 9. Circumferential variation of Sherwood number, $d = 8$ mm.

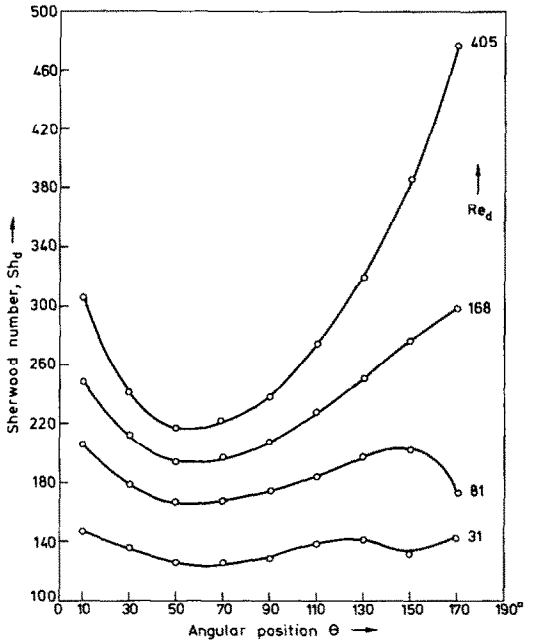

FIG. 10. Circumferential variation of Sherwood number, $d = 12$ mm.

5.1. *Local Sherwood number*

The distribution of Sherwood number around the hollow circumference (θ measured from the upstream lip of hollow) over a range of Reynolds number (Sh and Re are both based on the hollow diameter, d; viz. $Sh_d = kd/D$ and $Re_d = u_m d/\nu$) is depicted in Figs. 8–10 for hollow diameters 4, 8 and 12 mm re-

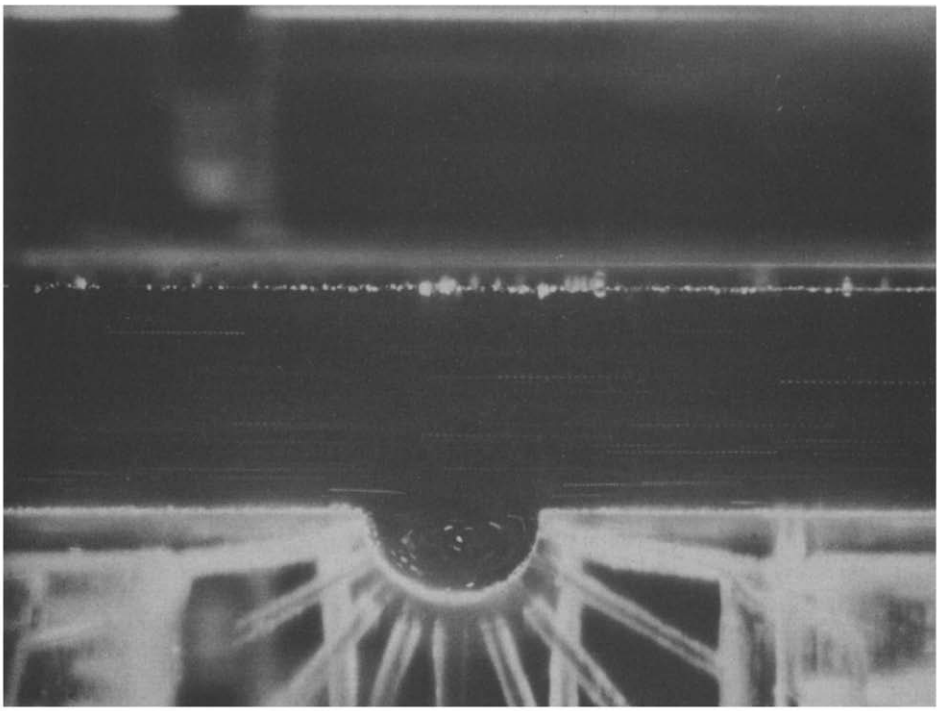

FIG. 11. Steady flow pattern in hollow, $Re_d = 100$.

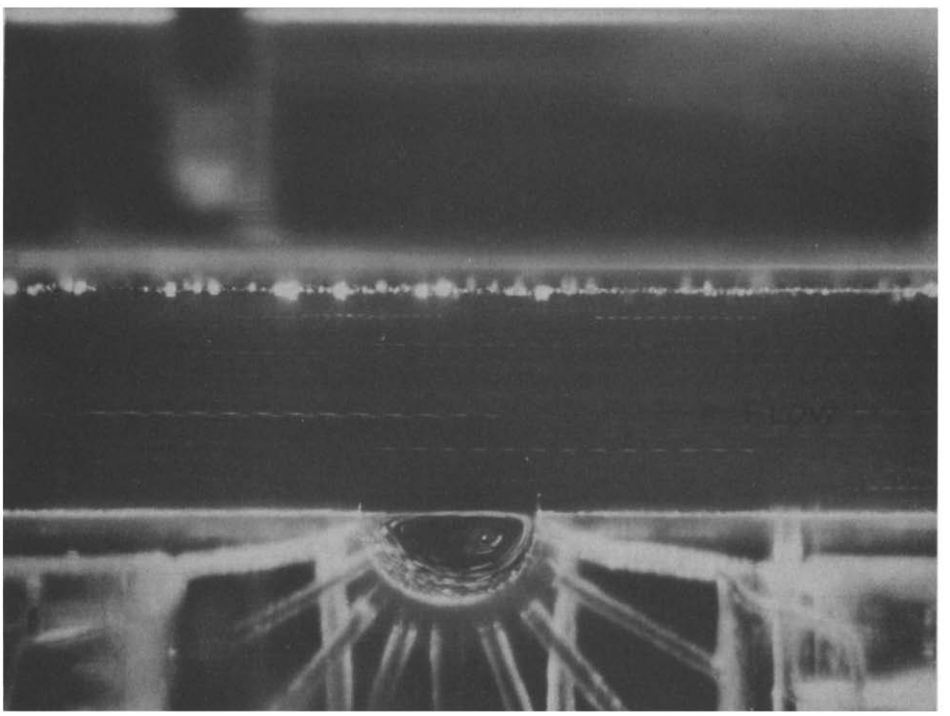

FIG. 12. Steady flow pattern in hollow, $Re_d = 400$.

spectively. The local Sherwood number first decreases with θ and then increases, the minimum value being generally achieved at around 60°; this variation is more pronounced at larger Reynolds number. For the 4 mm hollow, little variation in Sh_d is recorded except near the hollow lips where the Sherwood number rises sharply in all cases. This variation is more or less symmetrical about the axis which is to be expected from experimental particle photographs taken at low Reynolds number (i.e. at low flow rates for smaller size hollows). Figure 11 shows one such photograph at $Re_d = 100$ ($d =$ 8 mm) taken with polystyrene particles of about 125 μm diameter suspended in the flow. Clearly, the vortex centre is almost coincident with the hollow centre-line.

As the Reynolds number increases, the vortex centre shifts downstream as depicted in Fig. 12 at $Re_d = 400$; this results in streamlines lying closer to each other in the downstream quadrant than in the upstream one. One would therefore expect higher shear stresses in the downstream quadrant and hence higher Sherwood number as confirmed by Figs. 9 and 10. In the absence of any other experimental data, the qualitative agreement between the electrochemical mass-transfer measurements and the particle photographs is good.

The distribution of Sherwood number with Reynolds number is exhibited in Figs. 13 and 14 for all hollows tested at two typical angular positions, $\theta = 90°$ and 150°. For the 4 mm hollow, at $\theta = 90°$, the

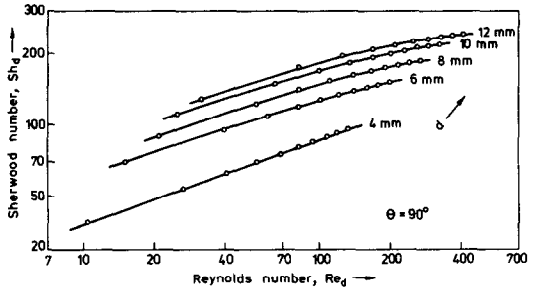

FIG. 13. Sherwood number vs Reynolds number, $\theta = 90°$.

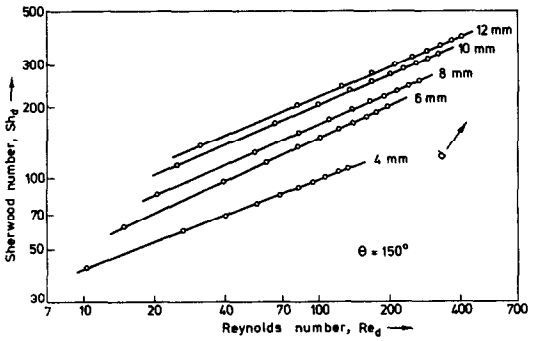

FIG. 14. Sherwood number vs Reynolds number, $\theta = 150°$.

variation is linear with a slope close to 1/3, as is the case in the absence of the hollow. For larger hollow sizes, one does not expect proportionate increase in Sherwood number at the hollow bottom ($\theta = 90°$) with increasing Reynolds number. At $\theta = 150°$, however, because the vortex centre shifts downstream with increasing Re_d, the rate of rise of Sh_d is greater and in fact, the variation is linear for all hollow sizes as depicted in Fig. 14.

A cross-plot of Figs. 13 and 14 appears in Fig. 15, which depicts the variation of Sherwood number with hollow diameter. At $Re_d = 30$, points for different θ-values cluster around one straight line having a slope of 2/3. At $Re_d = 130$, points for a given θ-value still fall on a straight line but its slope increases from about 0.56 at $\theta = 30°$ to about 0.78 at $\theta = 150°$, the average slope being still about 2/3.

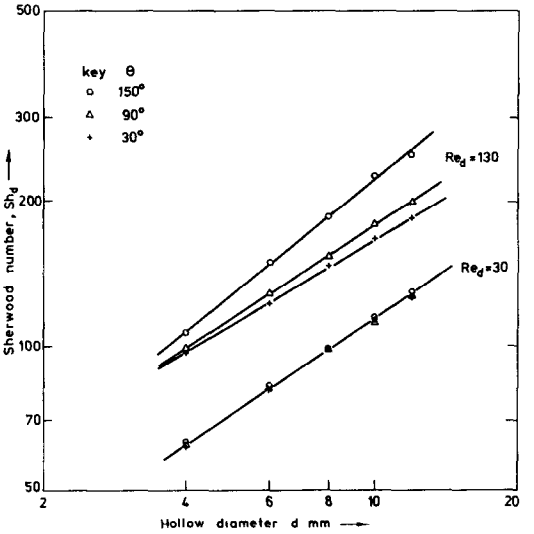

FIG. 15. Sherwood number vs hollow diameter.

5.2. *Average Sherwood number*

The average value $\bar{k}$ of the local values of mass-transfer coefficient over the hollow circumference was determined by integration of the measured local distribution. The variation of the average Sherwood number $\overline{Sh}_d = \bar{k}d/D$ with Re_d is plotted in Fig. 16 for all hollow sizes. Excellent straight line correlations are obtained with very little scatter and all lines have a slope of 1/3. It is therefore proposed that

$$\overline{Sh}_d = K(d)(Re_d Scb/L)^{1/3} \qquad (12)$$

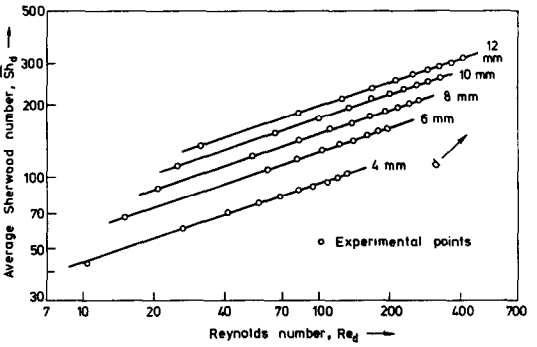

FIG. 16. Distribution of average Sherwood number.

where $K(d)$ is dependent only on the hollow diameter. In fact, the straight line plots of Fig. 16 yielded

$$K(d) = 1.40(d/2b)^{2/3}$$

again with very little scatter. Hence the following correlation has been obtained

$$\overline{Sh}_d = 1.40(Re_d Scb/L)^{1/3}(d/2b)^{2/3}. \qquad (13)$$

In view of equation (13), it was decided to base the Sherwood number and the Reynolds number on the channel height as opposed to the hollow diameter and a plot of $\overline{Sh}_b$ vs Re_b appears in Fig. 17. All the points lie on a single straight line which is

represented by the following equation.

$$\overline{Sh}_b = 0.70(Re_b Scb/L)^{1/3} \tag{14}$$

in which $\overline{Sh}_b = \bar{k}b/D$ and $Re_b = 2u_m b/\nu$. As the maximum deviation of any experimental point from this line is less than 2%, the data points have been omitted from the graph for clarity. It is most interesting to note that the hollow diameter does not appear in equation (14) and therefore, comparing with equation (11),

$$\overline{Sh}_b/Sh_0 = 0.76. \tag{15}$$

Clearly, on spatial-average basis, the local Sherwood number at the wall in steady flow is reduced by about a fourth due to the presence of the hollow.

expressed in terms of the local Sherwood number Sh_b by

$$c_f = \frac{2\tau}{\rho u_m^2} = 15.19\left(\frac{L}{b}\right)(Sh_b)^3 Sc^{-1} Re_b^{-2}. \tag{16}$$

Similarly the mean skin friction coefficient $\bar{c}_f$ for the hollow can be related to the channel wall skin friction coefficient c_{f_0} by

$$\frac{\bar{c}_f}{c_{f_0}} = \frac{\bar{\tau}}{\tau_0} = \left(\frac{\overline{Sh}_b}{Sh_0}\right)^3. \tag{17}$$

Here the average skin friction coefficient $\bar{c}_f$ within the hollow does in fact represent the same average as would be obtained, for instance, from a floating element skin friction gauge which extended the full

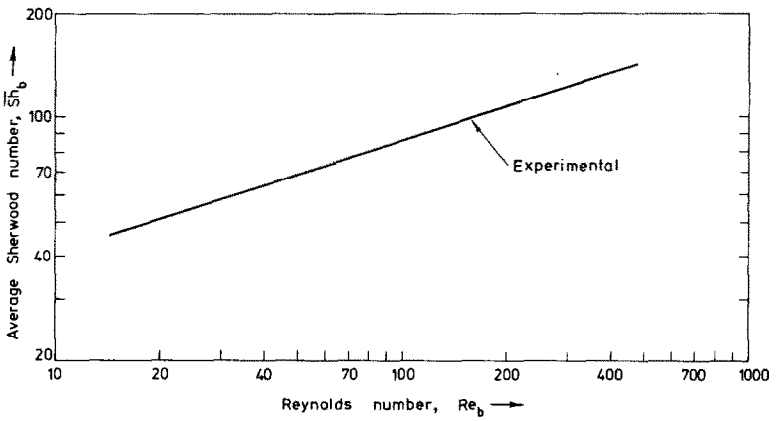

FIG. 17. Average Sherwood number in the presence of a hollow.

It is important to emphasize what these mass-transfer coefficients, as expressed in terms of Sherwood numbers, actually represent. In the case of the local Sherwood number, the mass-transfer coefficient is that which pertains to an isolated element of length L in the streamwise direction (in the case of a circular electrode, $L = 0.8136d_e$) imbedded in the wall of a channel or hollow which, except for the element, is impervious to mass transfer (assuming no interaction between adjacent electrodes). The average Sherwood number, given by equation (14) hence represents the mean of these local values, distributed around the hollow. This is not the same average as would have been obtained from a single mass-transfer electrode which extended the full circumference of the hollow ($L = \pi d/2$). In the case of the local measurements the concentration boundary layer begins afresh at each electrode, whereas for a single electrode of length $\pi d/2$ the concentration boundary layer would grow continuously from $\theta = \pi$ to $\theta = 0$. (Remember that the flow within the hollow is a recirculating flow.)

The most useful interpretation of the local Sherwood number is in terms of the local wall shear stress τ. It follows from equation (9) that the local skin friction coefficient c_f within the hollow can be circumference of the hollow. From equations (15) and (17) it can be seen that the average wall shear stress within the hollow is about 44% that of the channel wall. It is interesting to note that according to equations (14) and (17), the average skin friction coefficient within the hollow is proportional to Re_b^{-1} rather than $Re_b^{-1/2}$ as is the case with boundary-layer flows. Since c_{f_0} on the channel wall is likewise proportional to Re_b^{-1}, $(\overline{Sh}_b/Sh_0)$ is independent of Reynolds number.

To obtain the average overall mass-transfer coefficient for the hollow, we must return to the basic expression for the wall concentration gradient in the Lévêque approximation for the more general case where $s(x)$, the laminar flow velocity gradient at the wall, varies with streamwise distance x. It can be shown [21] that when the wall velocity gradient $s(x)$ is variable, and the wall concentration is zero, the local concentration gradient at the wall can be expressed as

$$\left(\frac{\partial c}{\partial y}\right)_x = \frac{c_0[s(x)]^{1/2}}{\Gamma\left(\frac{4}{3}\right)\left\{9D\int_0^x [s(t)]^{1/2}\,dt\right\}^{1/3}} \tag{18}$$

where c_0 is the bulk or free stream concentration,

and $\Gamma(4/3) = 0.8930$. The concentration boundary layer is assumed to begin at $x = 0$. If the local wall concentration gradient within the hollow is normalized by the value of channel wall concentration gradient $(\partial c/\partial y)_0$, we obtain

$$\frac{(\partial c/\partial y)_x}{(\partial c/\partial y)_0} = \frac{[s(x)/s_0]^{1/2}}{\left\{\frac{1}{x}\int_0^x \left[\frac{s(t)}{s_0}\right]^{1/2} dt\right\}^{1/3}} \tag{19}$$

where s_0 is the channel wall velocity gradient. In terms of the Sherwood number, the local wall concentration gradient within the hollow is given by

$$\frac{(\partial c/\partial y)_x}{(\partial c/\partial y)_0} = \frac{[Sh(x)/Sh_0]^{3/2}}{\left\{\frac{1}{x}\int_0^x \left[\frac{Sh(t)}{Sh_0}\right]^{3/2} dt\right\}^{1/3}} = \frac{[Sh(\theta')/Sh_0]^{3/2}}{\left\{\frac{1}{\theta'}\int_0^{\theta'} \left[\frac{Sh(\theta')}{Sh_0}\right]^{3/2} d\theta'\right\}^{1/3}} \tag{20}$$

where $\theta' = \pi - \theta$ is the angular position within the hollow measured from its downstream lip where the concentration boundary layer is assumed to originate.

The application of equation (20) can be illustrated by means of the data plotted in Fig. 18, which presents the variation of $Sh_b(\theta)/Sh_0$ within a 12 mm dia hollow for $Re_d = 290$. A curve was faired through the data points of Fig. 18, and the local values of $(\partial c/\partial y)_x/(\partial c/\partial y)_0$ obtained from equation (20) were averaged over the hollow circumference to obtain

$$\overline{(\partial c/\partial y)}_x/(\partial c/\partial y)_0 \cong 0.69.$$

Since the surface area exposed to the flow by the hollow is $\pi/2$ times the channel wall area which it replaced, the overall increase in mass transfer due to the presence of the hollow is only about 8% in this particular example. The data for other hollow diameters and Reynolds numbers given in Figs. 8, 9 and 10 could be similarly employed to obtain overall average mass-transfer coefficients for the cases presented in these figures. Since it was found that $\overline{Sh_b}/Sh_0$ was essentially constant, it may be anticipated that the values of $\overline{(\partial c/\partial y)}_x/(\partial c/\partial y)_0$ for these other cases will not differ significantly from the value obtained in the example just presented. One may conclude that, at least for a single hollow, the presence of a hollow in a channel wall increases only modestly the mass transfer under conditions of steady laminar flow in the range $Re \lesssim 400$. It is anticipated however that this increase would be considerably larger in the more interesting case of pulsatile flow. It is hoped that the present investigation can be extended to the pulsatile flow case.

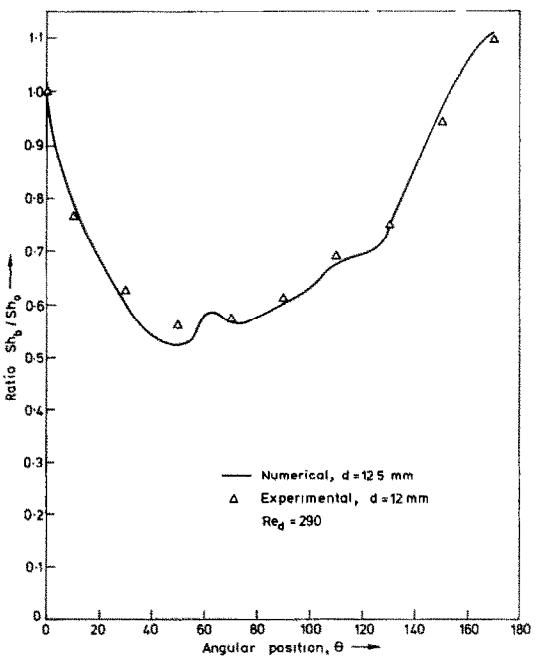

FIG. 18. Comparison with numerically-calculated Sherwood number.

6. DISCUSSION

It is perhaps appropriate to mention sources of probable errors which may have affected the results described in the preceding section. The largest source of error may be associated with the surface conditions in the vicinity of the electrode. Although great care was exercised in ensuring that the electrodes were mounted flush with the local surface curvature, after prolonged usage very small pockets were observed around some of the electrodes, where the electrolyte etched out the cement filler. On subsequent evaporation of the electrolyte from these tiny cavities, a white powder, presumably sodium hydroxide, was left behind. These cavities, if present may distort the flow locally. If a cavity communicates with the side of an electrode which thereby becomes exposed to the solution, the measured current will be higher. The test electrodes were inspected under a microscope before each run to ensure that they were in satisfactory condition.

As the electrode surface forms a part of the cylindrical hollow wall, it is not flat and its area is slightly (less than 1/3% in the worst case of a 4 mm dia hollow) larger than the calculated area based on the measured electrode diameter. In the derivation of equation (11), the curvature of the electrode surface was neglected to enable the assumption of linear velocity gradient in the concentration boundary layer to be made. However, the error introduced by this curvature must be small. In fact, a larger error may be expected due to the neglect of the axial diffusion term in the derivation of equation (11). For the very small electrodes used (typical diameter ~ 0.5 mm), this error may be significant in regions of very low shear stress, e.g. in the upstream quadrant of larger hollows at very low flow rates. According to Mizushina [17], if this effect is accounted for, equation (9) will be modified as follows:

$$\frac{kL}{D} = 0.807(sL^2/D)^{1/3} + 0.19(sL/D)^{-1/6}. \tag{21}$$

It can readily be shown that for $sL^2/D = 1000$, the error introduced by neglecting axial diffusion is less than 1% and even for sL^2/D as low as 100, this error is only just over 2%. It should be noted that all the sources of error mentioned above will result in an increase in the current measured. A source of error which usually results in a reduction of the measured current is the contamination of the electrode surface. This contamination is caused by the contamination of the solution (caused by exposure to light or absorption of atmospheric gases, etc.) and can be in the form of either an oxide film or a corrosion deposit. Although great care was taken, these effects could not be completely eliminated.

It is estimated that the overall uncertainty of any data point was less than 3%.

To the best of the authors' knowledge, no other data on shear stress or Sherwood number distribution around the circumference of a hollow are available. However, Snuggs and Aggarwal [22] have recently carried out a numerical study of flow in hollows. They integrated the Navier–Stokes equations using a fourth-order finite-difference method. Their calculations were extended to the present flow situation, and the wall vorticity (and hence shear stress) variation was computed for a 12.5 mm dia hollow, over a range of Reynolds number. Using the relationship $Sh_b/Sh_0 = (\tau/\tau_0)^{1/3}$, according to the Lévêque theory, the variation of Sh_b/Sh_0 with θ was calculated and this is shown in Fig. 18 for the particular case of $Re_d = 290$. The agreement with the experimental data is excellent.

7. CONCLUSIONS

An electro-chemical technique was utilized to measure local Sherwood numbers in semi-cylindrical hollows mounted in the base of a narrow channel. The flow in the channel at entry to the test section was steady, laminar and fully-developed and the Reynolds number varied from about 20 to 500. The electrolytic solution used was a redox couple consisting of equal quantities of potassium ferro- and ferricyanides dissolved in an excess of caustic solution. Nickel wires of nominal 0.5 mm dia, mounted flush with the surface at the points of measurement, were used as cathodes and a large strip anode was mounted in the furthermost downstream position. Current measurements were made under diffusion-controlled conditions. Measurements made in the absence of a hollow were in good agreement with well-known results. Current measurements in hollows led to the evaluation of local and average Sherwood numbers as functions of the Reynolds number and the hollow diameter. These are directly related to the local and average wall shear stress, and can be used to obtain local and average mass-transfer coefficients.

1. For a given hollow size, Sh_d usually exhibits a minimum value at around $\theta = 60°$. At very low Re_d values, the variation is almost symmetrical about the hollow axis because the vortex centre is almost coincident with the line of fore and aft symmetry. As Re_d increases, the vortex centre shifts slowly downstream and so the variation of Sh_d with θ is much more pronounced, especially in the downstream quadrant.

2. The variation of Sh_d with Re_d is almost linear on a log–log scale. This is particularly so for smaller hollows and at larger values of θ (say, $\theta > 120°$) for larger hollows. For $\theta < 120°$ and $d > 6$ mm, although the variation is linear at low Reynolds number, the increase becomes less rapid as Re_d is increased.

3. The variation of Sh_d with the hollow diameter appears to follow the relation,

$$Sh_d \propto d^a \tag{16}$$

where the exponent, a, is a function of the Reynolds number and the angular position, θ, within the hollow.

4. The average Sherwood number, taken over the hollow circumference, is correlated to the hollow diameter by equation (12). When the Sherwood number and Reynolds number are based on the channel height (rather than the hollow diameter), all the data points lie on a unique straight line defined by equation (14) in which the hollow diameter "d" does not appear at all, and it is found that the ratio of $\overline{Sh}_b$ to Sh_0 is constant (independent of Re_b or d) with a value of about 0.75, for the entire range of test conditions investigated.

5. The experimental variation of Sh_d with θ is compared with a numerical calculation for a 12.5 mm dia hollow over a range of Reynolds number. The agreement is found to be excellent.

Acknowledgements—The authors would like to thank Dr. W. S. Haworth of the Department of Engineering Science, Oxford for helping with titration experiments and Dr. B. J. Bellhouse for securing travel funds for one of the authors (L.T.) from Johnson and Johnson of U.S.A. Thanks are also due to the authors' technicians, Mr. G. Kershaw for his general help in the development of the project and Mr. C. Curl for designing and building the electronic circuits. Appreciation is expressed to Professor R. A. Seban, University of California, Berkeley, for many helpful discussions.

The research was supported by the Science Research Council and the National Science Foundation.

REFERENCES

1. T. Kolobow, W. Zapol, J. E. Pierce, A. F. Keeley, R. L. Replogle and A. Haller, Partial extracorporeal gas exchange in alert newborn lamb with a membrane artificial lung perfused via an A.V. shunt for periods up to 96 hours, *Trans. Am. Soc. Artif. Internal Organs* **14**, 328–334 (1968).
2. E. C. Peirce, Jr. and N. R. Dibelius, The membrane lung: studies with a new high permeability co-polymer membrane, *Trans. Am. Soc. Artif. Internal Organs* **14**, 220 (1968).
3. L. F. Mockros, *The Artificial Lung, Biomedical Engineering*, edited by J. H. V. Brown *et al.*, Chapter 12. Davis, Philadelphia (1971).
4. M. H. Weissman and L. F. Mockros, Oxygen transfer to blood flowing in coiled circular tubes, *J. Engng Mech. Div. Am. Soc. Civ. Engrs* **94**, 857–871 (1968).

5. M. M. Illickal, G. E. Brown, J. M. Van de Water, W. H. Lea, D. B. Pall and J. V. Maloney, Boundary layer phenomena in membrane oxygenators, *Surg. Forum* **18**, 134 (1967).
6. P. A. Drinker, R. H. Bartlett, R. M. Bialer and B. S. Noyes, Jr., Augmentation of membrane gas transfer by induced secondary flows, *Surgery* **66**, 775–781 (1969).
7. J. A. Benn, P. A. Drinker, B. Mikic, M. C. Shults, E. J. Lacava, G. S. Kopf, R. H. Bartlett and E. L. Hanson, Predictive correlation of oxygen and carbon dioxide transfer in a blood oxygenator with induced secondary flows, *Trans. Am. Soc. Artif. Internal Organs* **17**, 317–322 (1971).
8. B. J. Bellhouse, F. H. Bellhouse, C. M. Curl, T. I. MacMillan, A. J. Gunning, E. H. Spratt, S. B. MacMurray and J. M. Nelems, A high efficiency membrane oxygenator and pulsatile pumping system, and its application to animal trials, *Trans. Am. Soc. Artif. Internal Organs* **19**, 72–79 (1973).
9. J. M. Nelems, B. J. Bellhouse, C. M. Curl, T. I. MacMillan and S. B. MacMurray, Prolonged pulmonary support of newborn lambs with the Oxford membrane oxygenator, *Trans. Am. Soc. Artif. Internal Organs* **20**, 293–298 (1974).
10. J. R. Mitchell and C. J. Schwarta, *Arterial Disease*. Blackwells, Oxford (1965).
11. A. E. Bergles, Survey and evaluation of techniques to augment convective heat and mass transfer, in *Progress in Heat and Mass Transfer*, Vol. 1, pp. 331–422 (1969).
12. M. Eisenberg, C. W. Tobias and C. R. Wilke, Ionic mass transfer and concentration polarisation at rotating electrodes, *J. Electrochem. Soc.* **101**, 306–320 (1954).
13. P. Delahay, *New Instrumental Methods in Electrochemistry*. Interscience, New York (1954).
14. L. P. Reiss and T. J. Hanratty, Measurement of instantaneous rates of mass transfer to a small sink on a wall, *A.I.Ch.E. Jl* **8**, 245–247 (1962).
15. L. P. Reiss and T. J. Hanratty, An experimental study of the unsteady nature of the viscous sublayer, *A.I.Ch.E. Jl* **9**, 154–160 (1963).
16. F. M. White, *Viscous Fluid Flow*, p. 338. McGraw-Hill, New York (1974).
17. T. Mizushina, The electrochemical method in transport phenomena in *Advances in Heat Transfer*, edited by T. P. Irvine, Jr. and J. P. Hartnett, Vol. 7, pp. 87–161. Academic Press, New York (1971).
18. E. H. Swift, *A System of Chemical Analysis*. W. H. Freeman, San Françisco (1938).
19. S. L. Gordon, J. S. Newman and C. W. Tobias, The role of ionic migration in electrolytic mass transport; Diffusivities of $[Fe(CN)_6]^{3-}$ and $[Fe(CN)_6]^{4-}$ in KOH and NaOH solutions, *Ber. Bunsenges. Phys. Chem.* **70**(4), 414–420 (1966).
20. S. C. Ling, Heat transfer from a small isothermal spanwise strip on an insulated boundary, *J. Heat Transfer* **85**, 230–236 (1963).
21. M. J. Lighthill, Contributions to the theory of heat transfer through a laminar boundary layer, *Proc. R. Soc.* **A202**, 359–377 (1950).
22. T. A. Snuggs and J. K. Aggarwal, Steady and unsteady flow in a semi-cylindrical hollow, Oxford University Engineering Laboratory Report No. 1118/75 (1975).

MESURES ELECTROCHIMIQUES DE TRANSFERT MASSIQUE DANS DES CAVITES SEMI-CYLINDRIQUES

Résumé—On décrit des mesures des distribution circonférentielle du nombre de Sherwood local dans une cavité semi-cylindrique orientée perpandiculairement à l'écoulement principal, à la base d'un canal rectangulaire et étroit. Cette géométrie entre autres raisons, est intéressante par son application à l'équipement d'oxygénation du sang. Les conditions expérimentales sont telles que l'écoulement laminaire est dynamiquement établi à l'entrée de la cavité et les mesures couvrent un domaine de nombre de Reynolds de 20 à 500, basé sur le diamètre de la cavité et sur la vitesse moyenne du canal. On utilise une technique électrochimique avec un couple d'oxydo-réduction et des fils fins de nickel pour électrodes des mesures de courant, faites dans des conditions de réaction électroytique contrôlée par la diffusion, conduisent à l'évaluation du nombre de Sherwood. On présente graphiquement la distribution circonférentielle du nombre de Sherwood dans la cavité, en fonction du nombre de Reynolds de l'écoulement et de la taille de la cavité. Le nombre de Sherwood croît aussi bien avec le nombre de Reynolds qu'avec le diamètre de la cavité, mais il présente usuellement un minimum dans le quadrant amont. Le nombre de Sherwood, pris en moyenne sur la circonférence est déterminé et il conduit à une formule semblable à celle en l'absence de la cavité, à la différence près d'une constante plus faible. Les résultats sont comparés à des calculs numériques de Snuggs et Aggarwal pour la distribution du nombre de Sherwood dans la cavité et on trouve un excellent accord.

ELEKTROCHEMISCHE MESSUNGEN DES STOFFTRANSPORTS IN HALBKREISFÖRMIGEN RINNEN

Zusammenfassung—Es werden Messungen der über den Umfang verteilten örtlichen Sherwood–Zahlen in einer halbkreisförmigen Rinne beschrieben. Die Rinne verläuft quer zur Hauptströmungsrichtung in der Grundfläche eines engen, rechteckigen Kanals. Diese Geometrie ist *u. a.* deshalb interessant, weil sie in Apparaten zur Sauerstoffanreicherung von Blut Verwendung findet. Die Versuchsanordnung war so gewählt, daß am Eintritt in die Rinne eine hydrodynamisch voll ausgebildete, laminare Strömung vorlag. Die Messungen umfaßten einen Bereich der Reynolds–Zahl von ungefähr 50 bis 500, wobei die Reynolds–Zahl mit dem Öffnungsdurchmesser und der mittlern Strömungsgeschwindigkeit im Kanal gebildet wird. Es kam eine elektrochemische Technik zur Anwendung, bei der ein Redox–Paar den Elektrolyten enthielt und dünne Nickeldrähte die Versuchselektroden bildeten. Strommessungen, die unter den Bedingungen der durch Diffusion bestimmten elektrolytischen Reaktion gemacht wurden, führten zur Bestimmung der Sherwood–Zahl. Die Verteilung der Sherwood–Zahl über den inneren Umfang der Rinne wird als Funktion der Reynoldszahl der Strömung und der Öffnungsgröße grafisch dargestellt. Die Sherwood–Zahl nimmt sowohl mit der Reynolds–Zahl als auch mit dem Öffnungsdurchmesser zu, aber sie weist im allgemeinen irgendwo im stromaufwärts gelegenen Quadranten der Rinne ein Minimum auf. Die über den Umfang der Rinne gemittelte Sherwood–Zahl wurde berechnet und führte zu einer Korrelation, die bis auf einen kleineren Wert der Konstante derjenigen in Abwesenheit der Rinne entspricht. Die Ergebnisse wurden mit einer numerischen Berechnung der Verteilung der Sherwood–Zahl in der Rinne nach Snuggs und Aggarwal verglichen, wobei eine ausgezeichnete Übereinstimmung festgestellt werden konnte.

ЭЛЕКТРОХИМИЧЕСКИЕ ИЗМЕРЕНИЯ ПЕРЕНОСА МАССЫ В ПОЛУЦИЛИНДРИЧЕСКИХ ПОЛОСТЯХ

Аннотация — Проведены измерения тангенциального распределения локального числа Шервуда в полуцилиндрической полости, ориентированной поперек основного потока у основания узкого прямоугольного канала. Помимо других причин, эта геометрия интересна тем, что она используется в аппарате по обогащению крови кислородом. Экспериментальная часть смонтирована таким образом, что на входе в полость имеет место гидродинамически полностью развитое ламинарное течение, и измерения проводятся в диапазоне числа Рейнольдса от 20 до 500, отнесенного к диаметру полости и средней скорости течения в канале. Использовался электрохимический метод измерения, при котором электродами служат никелевые проволочки, образующие вместе с электролитом окислительно-восстановительную систему. Число Шервуда определялось по замерам тока при электролитической реакции, контролируемой диффузией. Приведен график тангенциального распределения значений числа Шервуда в полости в зависимости от числа Рейнольдса для потока и размера полости. Число Шервуда возрастало с увеличением числа Рейнольдса и диаметра полости, но всегда оставалось минимальным на начальном участке. Проведен расчёт числа Шервуда, осредненного по окружности полости, в результате чего получена зависимость, идентичная зависимости при отсутствии полости, за исключением более низкого значения постоянной. Результаты сравнивались с численными данными Снаггса и Аггарвала по распределению числа Шервуда в полости и получено очень хорошее соответствие.